EGG-CDAP-5419

May 1981

POR

FUEL PRESSURE SINTERING (FHOTPS)

NRC Research and Technical Assistance Report

R. E. Mason

U.S. Department of Energy
Idaho Operations Office • Idaho National Engineering Laboratory

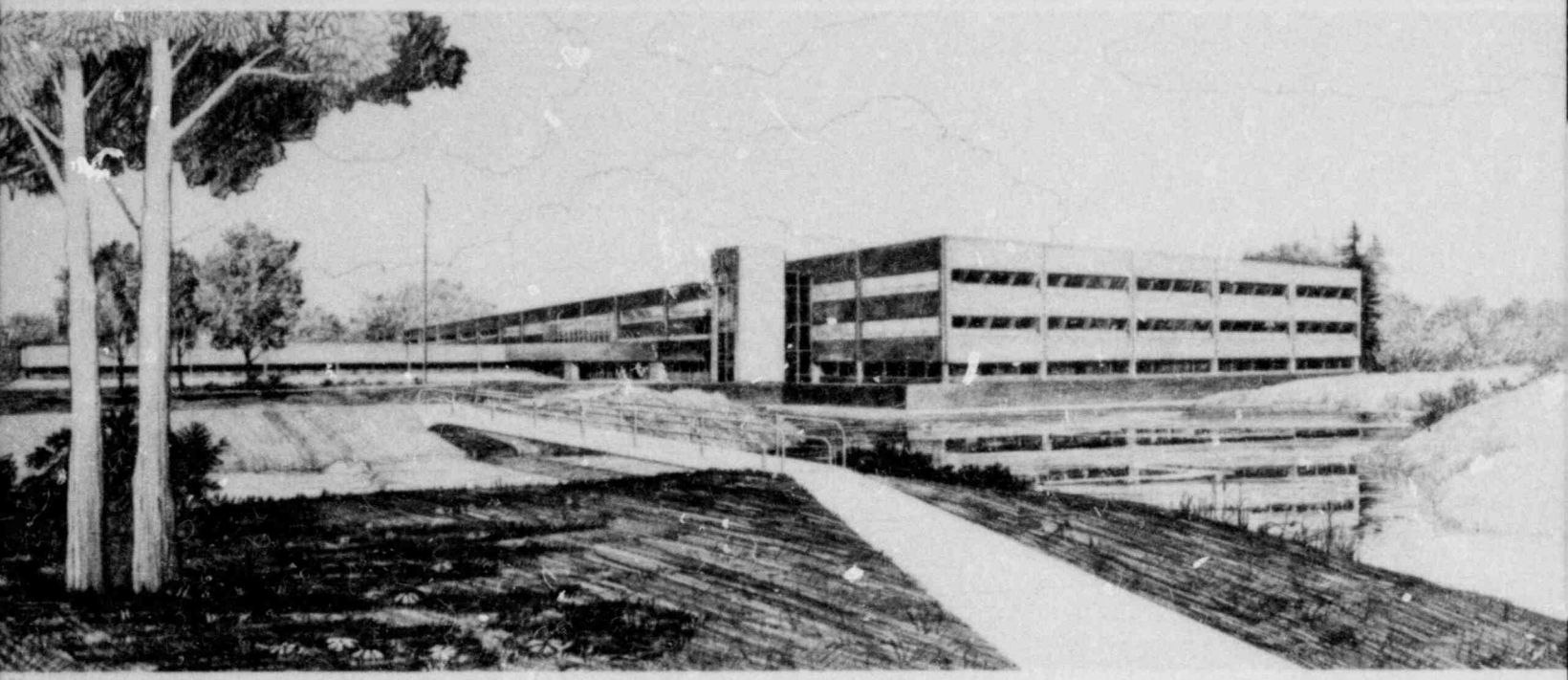

This is an informal report intended for use as a preliminary or working document

Prepared For:
U. S. Nuclear Regulatory Commission
Under DOE Contract No. DE-AC07-76ID01570
Fin. No. A6050

EG&G Idaho

EG&G Idaho, Inc.

FORM EG&G-398
(Rev. 11-79)

INTERIM REPORT

Accession No. _____

Report No. EGG-CDAP-5419

Contract Program or Project Title:
Fuel Behavior Model Development Program

Subject of this Document: Fuel Pressure Sintering (FHOTPS)

Type of Document: Internal Report

Author(s): R. E. Mason

NRC Research and Technical Assistance Report

Date of Document: May 1981

Responsible NRC Individual and NRC Office or Division: G. P. Marino - NRC-RSR

EG&G Idaho, Inc.
Idaho Falls, Idaho 83415

Prepared for the
U.S. Nuclear Regulatory Commission
Washington, D.C.
Under DOE Contract No. DE-AC07-76ID01570
NRC FIN No. A6050

INTERIM REPORT

FOREWORD

This report describes a model for pressure sintering (hot pressing) of urania or mixed oxide reactor fuels. The fuel hot pressing (FHOTPS) model is one of several materials properties models in the MATPRO handbook[a] used to calculate densification of reactor fuels. Densification of fuel affects heat transfer from the fuel pellet to the cladding, fission gas release rate and fuel-cladding interaction. Densification occurring because of applied stress (pressure sintering) as calculated by the FHOTPS model is to be added to the volume change calculated by the FUDENS and FSWELL models. The FUDENS and FSWELL models are based on in-pile data which may include some densification by pressure sintering. Densification by pressure sintering in their data base is, however, unresolvable from the volume change caused by irradiation.

This model will replace the FHOTPS model described in MATPRO-Version 11, Revision 1. The format and numbering scheme of the text are consistent with this intended use. The FHOTPS model was developed to calculate in-reactor pressure densification of light water reactor (LWR) fuel and will be utilized in the analytical Fuel Rod Analysis Program codes, FRAPCON-2[b] and FRAP-T6.[c]

---

a. D. L. Hagrman, G. A. Reymann, R. E. Mason, MATPRO-Version 11 Revision 1: A Handbook of Materials Properties for Use in the Analysis of Light Water Reactor Fuel Rod Behavior, NUREG/CR-0497, TREE-1280, Rev. 1, February 1980.

b. G. A. Berna et al., FRAPCON-2: A Code for the Calculation of Steady State Thermal-Mechanical Behavior of Oxide Fuel Rods, NUREG/CR-1845, December 1980.

c. L. J. Siefken et al., FRAP-T6: A Computer Code for the Transient Analysis of Oxide Fuel Rods, NUREG/CR-2148, EGG-2104, May 1981.

The proposed FHOTPS model is different from the hot pressing model described in the FRAP-T6 code user's manual. The FRAP-T6 hot pressing model does not consider only hot pressing (although called a hot pressing model). Rather, it is a gross correlation of data from the Power Burst Facility and Halden Test Reactor which includes volume change by thermal sintering, hot pressing, irradiation densification, crack healing and creep densification processes. The stress dependence of the FRAP-T6 hot pressing model is superficial.

The proposed hot pressing model calculates the fractional volume change rate of fuel under hydrostatic pressure and elevated temperatures. It models the removal of closed porosity and porosity created by released fission gases. The model does not calculate volume changes resulting from crack healing because the number of contact points (which can only be modeled statistically) will be more rate controlling than the relatively fast sintering rates.

CONTENTS

FIGURES

TABLES

9. FUEL PRESSURE SINTERING (FHOTPS)

(R. E. Mason)

Urania or mixed oxide fuel pellets densify when exposed to sufficiently nigh nydrostatic pressures (pressure sintering), nigh temperatures (thermal sintering) and/or irradiation. This report discusses a densification model based on published out-of-pile fuel pressure sintering data. The pressure sintering model complements the irradiation dependent densification model described in Section A-7 of the MATPRO nandbook.[A-9.18]

A summary of the pressure sintering model, FHOTPS, is contained in Section 9.1. Section 9.2 describes pressure sintering theories and examines their applicability to model urania and mixed oxide pressure sintering data. Section 9.3 describes the develooment of the FHOTPS model, provides standard error estimates and compares FHOTPS calculated results with experimental data. Section 9.4 gives the FORTRAN computer program listing of the FHOTPS model, and the references are given in Section 9.5.

9.1 Summary

Fuel densification in a reactor environment is a function of temperature, stress and irradiation. Temperature and stress densification mechanisms are driven by a stress, P, expressed by

$$P = P_e - P_i + \frac{2\gamma}{a} \qquad \text{(A-9.1)}$$

where

P_e = external nydrostatic stress (Pa)

P_i = internal pore pressure (Pa)

γ = surface energy per unit area (J/m^2)

a = grain size (m).

Pressure sintering is the dominant densification process if the stress $(P_e - P_i)$ is much larger than the surface energy stress, $2\gamma/a$. Densification of in-pile fuel will be dominated by an external hydrostatic stress, P_e, when present, because the internal pore pressure, P_i, and the surface energy stress, $2\gamma/a$, are generally much smaller than the externally applied stress. Over an extended irradiation period and at zero P_e, the internal pore pressure, P_i, could cause fuel swelling and the surface energy stress could cause some fuel densification. However, these changes in fuel volume are small compared with densification caused by applied stress and are not considered in the development of the FHOTPS model.

Equation (A-9.1) does not include an irradiation related driving stress. It is assumed that the irradiation densification driving stress would be added to the right side of Equation (A-9.1). Since the irradiation densification driving stress is a linear term, it is treated independently as a separate model. This is the FUDENS model of MATPRO 11, Revision 1. The values calculated with the FUDENS model should, therefore, be added to the FHOTPS model described in this section. The reader should, however, be cautioned that data used to develop the FUDENS model were in-pile data which may include some pressure sintering effects so that combining the two model outputs may be conservative. There are no in-pile data available that will allow separation of these effects.

A lattice diffusion creep equation was fit to the data of Solomon et al., [A-9.1] to give the equation used for urania in the FHOTPS model,

$$\frac{1}{\rho}\frac{d\rho}{dt} = 48939\left(\frac{1-\rho}{\rho}\right)^{2.7}\frac{P}{TG^2}\exp\left(Q_u/RT\right) \qquad \text{(A-9.2)}$$

where

t = time (s)

T = temperature (K)

G = grain size (μm)

R = 8.314 (J/mole*K)

Q_u = activation energy (J/mole)

ρ = fraction of theoretical density (unitless)

p = hydrostatic pressure (Pa).

The activation energy of urania pressure sintering for Equation (A-9.2) is calculated with the oxygen-to-metal dependent equation

$$Q_u = R\left\{9000 \exp\left[\left(\frac{20 - 8|\log (x - 1.999)|}{|\log (x - 1.999)|} + 1.0\right]^{-1} + 36294.4\right\} \quad \text{(A-9.3)}$$

where

x = oxygen-to-metal ratio.

The lattice diffusion creep equation was fit to the mixed oxide data of Routbort et al.,[A-9.2] to give the mixed oxide fuel pressure sintering equation,

$$\frac{1}{\rho}\frac{d\rho}{dt} = 1.8 \times 10^7 \left(\frac{1-\rho}{\rho}\right)^{2.25} \frac{p}{TG^2} \exp \frac{-450000}{RT} . \quad \text{(A-9.4)}$$

The standard error of estimate for both equations is ±0.5% of the calculated density.

Care must be exercised when using these models out of the 1600 to 1700 K and 2 to 6 MPa data base range. Pressure sintering not represented in the data base may be controlled by a different creep densification mechanism, as discussed below. Pressure sintering rates would then be much different than those calculated by Equations (A-9.2) or (A-9.4).

9.2 Pressure Sintering Process and Data

Pressure sintering or volume creep consists of several modes of creep. One of these modes or creep mechanisms can dominate the others depending on the fuel temperature, pressure, porosity, and grain size conditions as will be discussed below. Equations representing each creep mechanism combined with the theoretical constants of UO_2 were used by Routbort et al.,[A-9.2] to determine the most probable dominating (contributes the highest densification rate) mechanism under reactor operating conditions. These equations, their use and the published experimental data used to develop the FHOTPS model are described in this section.

9.2.1 Creep Densification

Several distinct mechanisms are observed which contribute to fuel densification. These are lattice diffusion (Narbarro-Herring creep), or rate independent plasticity (yielding or dislocation glide).[A-9.3] Each mechanism imposes specific stress-porosity-temperature dependent functions. One or any combination of these creep mechanisms can dominate densification depending on the grain size-stress-porosity-temperature conditions. There is no single mechanism which will always dominate the densification process. Therefore, an equation representing each mechanism is presented to indicate the densification parameter dependencies possible.

Pressure sintering by grain boundary diffusion creep (grain boundary acting as a diffusion path) is usually dominant at temperatures less than one half the melting temperature.[A-9.3, A-9.4] The densification rate by grain boundary creep is expressed by

$$\frac{d\rho}{dt} = \frac{4.5\ \delta\ D_b\ \Omega}{kT\ b^3} \frac{P}{1-(1-\rho)^{1/3}} \qquad \text{(A-9.5)}$$

where

δ = grain boundary thickness

D_b = grain boundary diffusion coefficient

Ω = atomic volume

ρ = fraction of theoretical density

t = time

T = temperature

P = applied stress

k = Boltzman's constant

b = grain size.[a]

Pressure sintering by grain boundary diffusion creep can dominate only if the grain sizes remain small so that the diffusion paths along the grain boundaries are small.

Pressure sintering by lattice diffusion creep often dominates at temperatures greater than half the melting temperature and before significant grain growth has occurred. Densification by lattice diffusion creep is expressed by

---

a. It was assumed in this and the following equations that the effective particle radius is the grain size. This is consistent with the model which is based on the assumption of about one pore to every grain in the compact.

$$\frac{d\rho}{dt} = \frac{3D_v \Omega P}{kT\, b^2} \qquad \text{(A-9.6)}$$

where

D_v = lattice diffusion coefficient.

This equation is used to calculate densification by vacancy flow from the surface of a pore to sinks on nearby grain boundaries.[A-9.3]

Pressure sintering by power law creep can dominate at high fuel temperatures and/or pressures. Densification by power law creep (dislocation creep) has been derived by Wilkinson and Ashby[A-9.4] and by Wolf and Kaufman.[A-9.5] The densification rate equation is

$$\frac{d\rho}{dt} = \frac{SA}{T}\exp\left(\frac{Q}{kT}\right)\left\{\frac{\rho\,(1-\rho)}{\left[1-(1-\rho)^{1/n}\right]^n}\right\}\left(\frac{3|p|}{2n}\right)^n \qquad \text{(A-9.7)}$$

where

S = sign of pressure

n = stress and porosity exponent

A = constant

Q = power law activation energy (J/mole).

Equation (A-9.7) assumes steady state creep and densification independent of the grain size and is valid even after extensive grain growth.

The fourth pressure sintering mechanism, plastic flow, operates at low temperatures or very high strain rates and is defined by the expression

$$\frac{d\rho}{dt} = \left\{ \begin{array}{l} 0 \text{ if } \rho \geq 1\text{-}\exp\left(\frac{-3}{2}\frac{P}{\sigma_y}\right) \\ \infty \text{ if } \rho < 1\text{-}\exp\left(\frac{-3}{2}\frac{P}{\sigma_y}\right) \end{array} \right\} \qquad \text{(A-9.8)}$$

where

ρ = fraction of theoretical fuel density

σ_y = yield stress.

Densification by the plastic flow mechanism is assumed to occur instantaneously.[A-9.3]

The stress dependency of the above equations have been shown by Rossi and Fulrath,[A-9.6] McClelland,[A-9.7] Fryer,[A-9.8] and Wolf[A-9.5] to be dependent on the applied stress and the fuel porosity. Porosity in the fuel increases the stress in the vicinity of the pores and results in a vacancy concentration difference between the pore surfaces and the grain boundaries. Various porosity dependent functions have been proposed by the above authors but the porosity dependent function of Fryer[A-9.8] is the most generally accepted effective stress-porosity dependent function. The form of Fryer's expression is

$$P = \left(\frac{1-\rho}{\rho}\right)^n \qquad \text{(A-9.9)}$$

where

P = effective stress

ρ = fractional density

n = 1.0.

Routbort et al.,[A-9.2] found that the porosity exponent, n, of Equation (A-9.9) was not constant for mixed oxides but varied with the pressure sintering temperature. Routbort et al., mapped pressure sintering of mixed oxides (determined the most dominant mechanism using theoretical

material properties) but used predominately urania material constants. They found the lattice diffusion mechanism to dominate under light water reactor conditions (fuel temperatures between 1100 K and 3136 K, pressures less than 100 MPa and fuel densities greater than 0.90% of theoretical density). This conclusion, however, must be exercised with caution because the densification rate equations also depend on the grain size and the oxygen-to-metal ratio and neither were included in the pressure sintering map analysis. The oxygen-to-metal ratio has been shown by Seltzer et al.,[A-9.9, A-9.10, A-9.11] to strongly influence the activation energy and thereby drastically alter the densification rates predicted by Equations (A-9.5), (A-9.6) and (A-9.7).

The final pressure sintering mechanism is lattice diffusion modified to include an effective applied stress. The expression describing this mechanism is

$$\frac{1}{\rho}\frac{d\rho}{dt} = A\left(\frac{1-\rho}{\rho}\right)^{n}\frac{P}{TG^{2}}\exp\left(Q/RT\right) \qquad \text{(A-9.10)}$$

where

A = constant

Q = activation energy.

9.2.2 Pressure Sintering Data

The model presented in the summary is based on data published in the open literature which deals with final stage sintering of urania and mixed oxide fuels. The models are based on the urania pressure sintering data of Solomon et al.,[A-9.1] and the mixed oxide pressure sintering data of Routbort et al.[A-9.2] Other data are used as comparison data. Fuel resintering data or final stage sintering data are used because these data most closely resemble what is occurring in a reactor. Measurement techniques and urania and mixed oxide data published in the open literature are presented in this section.

9.2.2.1 Measurement Techniques. Immersion density and specimen length changes are used to obtain densification data. Immersion density is the more accurate technique, but only the initial and final densities are obtained. Densities from specimen length changes provide time-density data and are calculated using the equation

$$\frac{\rho}{\rho_f} = \left(\frac{\ell_f}{\ell}\right)^3 \qquad \text{(A-9.11)}$$

where

ρ = initial fraction of theoretical density (unitless)

ρ_f = final fraction of theoretical density (unitless)

ℓ_f = final length (mm)

ℓ = initial length (mm).

Density changes determined from length change measurements have, however, several inherent sources of error. The most critical error is the apparent length change caused by the test sample seating and/or changing alignment during the initial densification. This strain error is highly variable and only affects the initial 1 to 2% of sample densification. Creep (non-volumetric strain) of the sample and loading column is also a source of error. Routbort et al., however, measured final sample immersion densities and final densities from length change calculations and found only about 5% difference between the two techniques.

9.2.2.2 Urania Densification Data. Pressure sintering data of UO_2 fuel have been published by Solomon et al.,[A-9.1] Kaufman,[A-9.12] Amato et al.,[A-9.13] Hart,[A-9.14] Fryer,[A-9.8] and Warren and Chalklader.[A-9.15] The data of Solomon et al., and Kaufman are resintering data, whereas the data of Amato et al. are fabrication sintering data.

Solomon et al. measured pressure sintering rates of UO_2 fuel pellets which were thermally sintered at 1783 K for 3 hours to obtain pretest sample densities between 92 and 94% of theoretical density (TD). Pressure sintering tests were performed at 1673 K for up to 136 hours. Since the urania samples were presintered at 100 K above the pressure sintering temperature, there should be only a small thermal sintering contribution to the pressure sintering rates. Immersion densities of pretest samples were obtained with an accuracy of ± 0.5%. Sample integrity was maintained by slowly ramping to the test temperature (1673 K) and then cycling through various temperature-pressure test combinations. Experimental temperatures are reported to be accurate to within ±1 K and pressures are accurate to within 0.1%. A summary of experimental conditions is provided in Table A-I. The pressure sintering tests of Solomon et al. indicate that (a) significant densification occurred prior to application of pressure, (b) internal pore pressures were possibly influencing the densification rate, (c) pressure sintering rates are approximately linear with applied stress ($\sigma^{1.03}$ to $\sigma^{1.2}$) and (d) the activation energy for specimens at different temperatures and constant density was 0.290 MJ/g•mole. Solomon et al., however, determined that an activation energy of 0.480 MJ/g•mole obtained from two isothermal tests to be more accurate. Pressure cycling tests also showed that the specimens swelled after the applied pressure was removed and that the applied pressure-densification and released pressure-swelling rates were essentially reversible.

Kaufman[A-9.12] reported urania pressuring data of fuel at initial densities of between 80.7 and 83.7% TD. Immersion densities were taken both before and after pressure sintering with a ± 0.2% accuracy. Their data are intermediate sintering data and can only be used to check the FHOTPS model densification rates. The pellets used by Kaufman were sintered at a temperature 100 K less than the test temperature, but were sintered for a relatively long time. Thermal sintering contributions should, therefore, be very similar to the Solomon et al. data. Pressure sintering was performed in a single action graphite die lined with a tungsten foil to minimize the reaction of uranium with the carbon. The uranium reaction was also minimized by pressing in a 10^{-3} Torr

TABLE A-9.I. PRESSURE SINTERING DATA

		Presintering		Pressure Sintering						
Reference	Oxygen-to-Metal Ratio	Temperature (K)	Time (h)	Theoretical Density (%)	Temperature (K)	Time (s)	Pressure (MPa)	Stress Exponent	Porosity Exponent	Initial Grain Size (mm)
URANIA DATA										
Solomon[A-9.1]	2.004 + 0.001	1783 ± 1	3	92 to 98	1673 ± 1	$0<t<5\times10^5$	--	$1.03<n<1.2$	2.7	3.354
Kaufman[A-9.12]	--	2023	12-24	80 to 92	2123	--	3.86 to 3.96×10^7	--	--	10-40
Amato[A-9.13]	2.00	--	--	68 to 96	1373-1473	$900<t<3600$	2.76 to 5.52×10^7	--	--	--
MIXED OXIDE DATA										
Routbort[A-9.2]	1.98 + 0.01[a]	--	--	90 to 99	$1598 \leq T \leq 1823$	--	7.6 to 76	1.33	2.25	8.0

a. Mixed oxide pellets consisted of 25 weight percent Pu_2O_2 and 75 weight percent UO_2 (20% U235 enriched).

atmosphere. Reaction of the urania with the tungsten foil and the graphite die may have occurred, but the extent of influence is undetermined. Temperature control was within ± 1 percent. Kaufman observed no densification from heating prior to the application of the load. Kaufman found stress exponent values for Equation (A-9.9) between 1 and 4.5.

Amato et al.[A-9.14] also used a graphite die plunger lined with alumina to obtain hot pressing data. Pressure sintering tests were performed using a vacuum of 10^{-5} Torr. Test conditions are listed in Table A-9.I. The Amato et al. data are also intermediate sintering data plus final stage sintering data. Therefore, the data can only be used to check the densification rates and not used as part of the FHOTPS data base. Amato et al. indicated that trapped gases were affecting the densification rate but data backing this conclusion was not reported.

Fabrication pressure sintering data were reported by Hart[A-9.14] and Fryer.[A-9.8] These data include initial, intermediate and final stage densification. Since densification rate equations will change for each stage, these data are not useful in the MATPRO modeling effort. Reaction sintering (sintering while the components are chemically reacting) data were reported by Warren and Chalklader.[A-9.15] These data are not appropriate for use in the MATPRO modeling effort for the reasons listed above plus the fact that the chemical reaction affects the sintering process.

9.2.2.3 Mixed Oxide Densification Data. The results of the Routbort et al.,[A-9.2] and Voglewede[A-9.16, A-9.17] for mixed oxide pressure sintering data are the only data published in the open literature. Their mixed oxide samples consisted of 15 weight percent PuO_2 and 75 weight percent UO_2. Tests consisted of presintering each sample to an equilibrium density of approximately 90% TD in a double action punch and tungsten die and then applying additional temperature and pressure to evaluate pressure sintering rates. Immersion densities were obtained before and after each test, and specimen length changes were measured during the test. Pressure sintering data were found to be reproducible to

within ±20%. Detailed test conditions for the Routbort et al. data are provided in Table A-9.I. Routbort et al. found the porosity exponent ranged from 1.5 at 1673 K to 2.25 at 1823 K. Pressure sintering was also shown to be a nonlinear function of stress with a stress exponent of 1.33.

9.3 Model Development and Uncertainties

The pressure sintering model, FHOTPS, calculates the volume reduction rate of fuel under hydrostatic pressures and elevated temperatures. The model is based on the urania and plutonia data described above and the semiempirical equation suggested by Solmon et al., and Routbort and Voglewede. The model simulates the removal of closed porosity developed during fuel pellet fabrication and/or porosity created by released fission gases.

The appropriate pressure sintering mechanism to model reactor fuel behavior is best determined by comparing the densification rates calculated with the theoretical equations of Section 9.2. The equation indicating the largest densification rate at expected reactor pressures and temperatures is the best model for in-reactor pressure sintering. Routbort et al. performed this analysis for mixed oxides but used mostly UO_2 physical constants. Lattice diffusion was determined to be the controlling mechanism. A similar conclusion was reached by Solomon et al., in their analysis of urania densification rates. The lattice diffusion equation is therefore used as the framework equation for the final FHOTPS equations.

Equation (A-9.2) was obtained by fitting Equation (A-9.10) to the data of Solomon et al. Determining the constant A of Equation (A-9.10) constituted equation fitting to the data. Trial and error adjustments of A were made until the standard error of estimate from Equation (A-9.10) and the data converged to the smallest error possible. The porosity exponent, n, for urania was obtained by using the average slope value of $1/\rho(d\rho/dt)$ plotted versus $\ln [(1-\rho)/\rho]$. The average slope value was determined to be 2.7.

Equation (A-9.10) was fit to the Solomon et al. data using a porosity exponent of 2.7, an initial grain size of 3.5 μm, an assumed activation energy of 0.48 MJ/mole, and the reported hydrostatic pressure and isothermal temperature. This fitted equation, however, calculates a greater densification rate than indicated by the data of Amato et al. This is opposite to the expected calculational results since intermediate sintering is expected to be faster than final stage sintering. The lattice diffusion equation was therefore refit to the Solomon et al. data using an apparent activation energy closer to the 0.290 MJ/mole apparent activation energy obtained by Solomon et al. from specimen data taken at different temperatures. The activation energy used in the urania pressure sintering model is calculated with Equation (A-9.3). This equation and resulting calculated activation energy were used to be consistent with the FCREEP model of the MATPRO package. With the oxygen-to-metal ratio of 2.004, an apparent activation energy of 0.332 MJ/mole is calculated with Equation (A-9.3). This is relatively close to the lower Solomon et al. activation energy. Using this activation energy, Equation (A-9.10) was fit by trial and error adjustments of constants to fit the Solomon et al. data. A final error of estimation of ± 0.48% was obtained. Calculations using Equation (A-9.2) compared with data of its data base are shown in Figure A-9.1.

The mixed oxide pressure sintering rate equation suggested by Routbort et al. was used as the FHOTPS mixed oxide model except that the grain size dependence of the theoretical lattice diffusion equation was included to be consistent with the urania model. The 0.4 MJ/mole activation energy for mixed oxides suggested by Routbort et al., with an oxygen-to-metal ratio of 1.98, was used in the model. This activation energy is assumed not to vary with the oxygen-to-metal ratio because of a lack of data. The porosity exponent is also assumed constant at 2.25 which is the value determined by Routbort et al., for samples tested at 1823 K. Although Routbort et al. observed a temperature dependence of the porosity exponent, a model for the dependence was not developed because the data on which this conclusion is based was not included in the published report.

Equation (A-9.10) was fit to the Routbort et al. data using an activation energy of 0.4 MJ/g mole, a porosity exponent of 2.25, and an initial grain size of 9 μm. Constants were adjusted until the smallest standard error estimate was obtained. The final standard error of estimation is 0.5%. Figure A-9.2 shows a comparison of the mixed oxide densification rates calculated with the FHOTPS model which correspond with the Routbort et al. data.

The FHOTPS model calculates a density change rate. These calculations are easily modified to obtain strain rate by multiplying the calculational results by -1/3. This is a result of the following analysis. Using a fuel mass, g, a change in density can be expressed by

$$\frac{1}{\rho}\frac{d\rho}{dt} = \frac{\frac{g}{V} - \frac{g}{V_o}}{\frac{g}{V_T}}\frac{1}{\Delta t} \qquad \text{(A-9.12)}$$

where

V = final volume

g = Fuel mass

V_o = initial volume

V_T = volume of the mass, g, at theoretical density

Δt = time step.

Eliminating g and multiplying denominator and numerator by V_T gives

$$\frac{1}{\rho}\frac{d\rho}{dt} = V_T\left(\frac{V_o - V}{V\,V_o}\right)\frac{1}{\Delta t}. \qquad \text{(A-9.13)}$$

Assuming that $V_T = V$, then Equation (A-9.13) relates a densification strain rate to a volume strain rate of

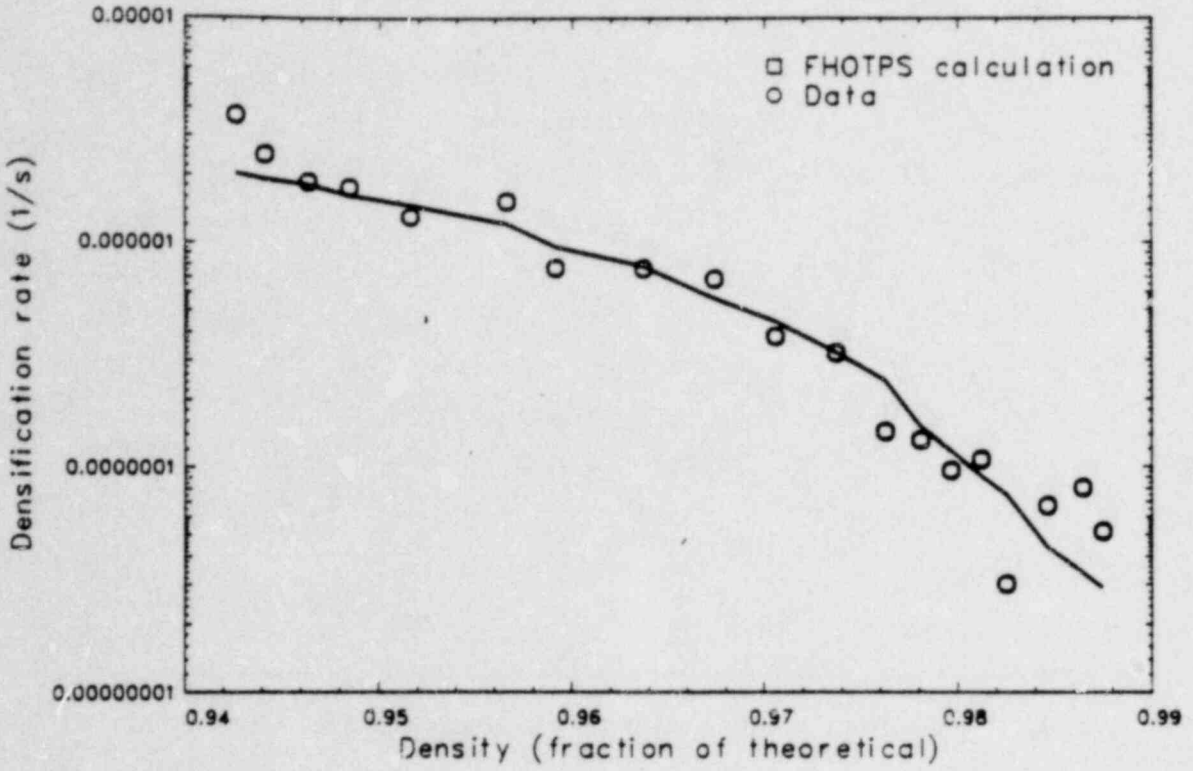

Figure A-9.1 Urania pressure sintering rates calculated using the FHOTPS model compared with data.

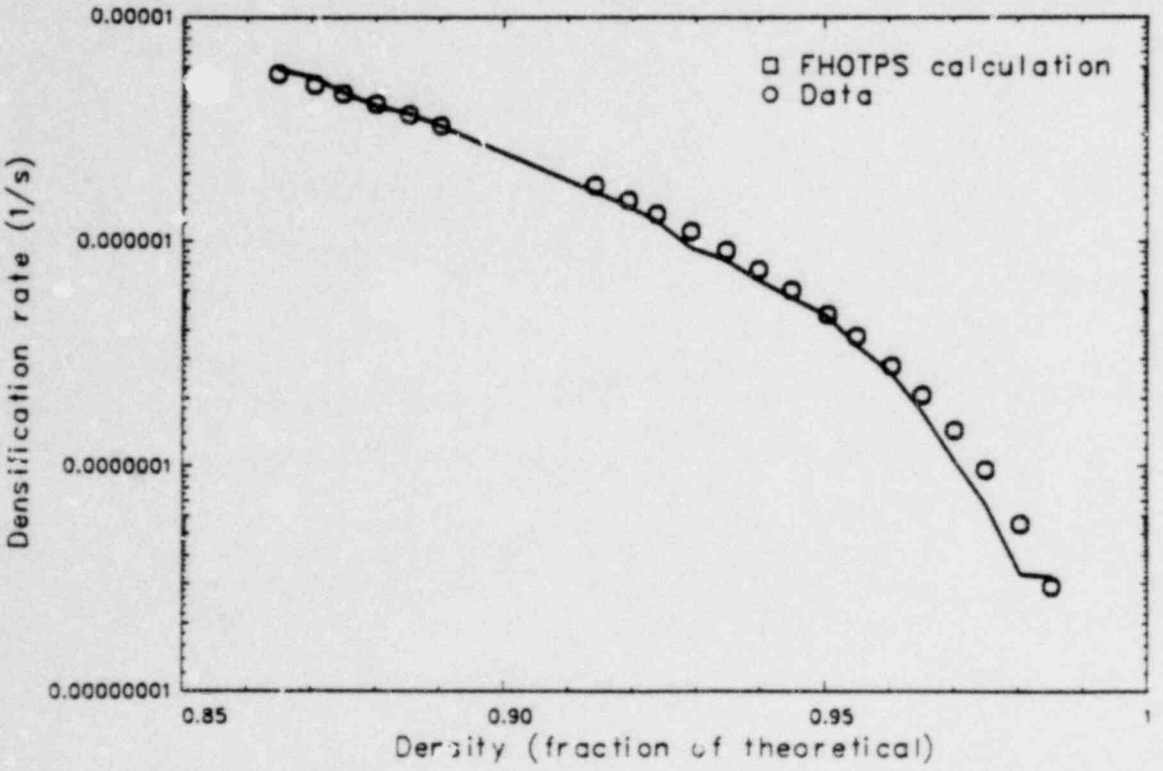

Figure A-9.2 Mixed oxide pressure sintering rates calculated using the FHOTPS model compared with data.

$$\frac{1}{\rho}\frac{d\rho}{dt} = \left(\frac{V - V_o}{V_o}\right)\frac{1}{\Delta t} \quad . \tag{A-9.14}$$

This can be reduced to a linear strain rate by the usual assumption that

$$\frac{1}{3}\frac{\Delta V}{V_o \Delta t} = \frac{\Delta L}{L_o}\frac{1}{\Delta t} \quad . \tag{A-9.15}$$

Equations (A-9.2) and (A-9.4) must be used with caution because the models are based on very limited data. Both equations are based on one data set, and these data cover only a small portion of the temperatures, pressures, oxygen-to-metal ratios, and grain sizes possible in a reactor environment. An additional concern is that a significiant change in any one of these parameters could result in a different creep mechanism.

9.4 Subcode FHOTPS FORTRAN Listing

Table A-9.II is a listing of FHOTPS model described above.

TABLE A-9.II. LISTING OF THE FHOTPS SUBCODE

```
      FUNCTION FHOTPS(COMP, FTEMP, HSTRES, GRNSIZ, FOM, RO)
C
C     FHOTPS = OUTPUT FRACTIONAL VOLUME CHANGE RATE FOR UO2 OR MIXED
C     OXIDES(CHANGE IN DENSITY / (INITIAL DENSITY * SECONDS)).
C
C     COMP   = INPUT PLUTONIA CONTENT (WEIGHT PERCENT).
C     FTEMP  = INPUT TEMPERATURE OF THE FUEL (K).
C     HSTRES = INPUT HYDROSTATIC STRESS ON THE FUEL PELLET (PA).
C     GRNSIZ = INPUT INITIAL GRAIN SIZE (MICRONS).
C     FOM    = INPUT FUEL OXYGEN TO METAL RATIO (UNITLESS).
C     RO     = INPUT FRACTIONAL FUEL DENSITY(UNITLESS).
C
C     THE DENSIFICATION CALCULATED WITH THIS FUNCTION IS BASED ON
C     DATA FROM THE FOLLOWING REFERENCES.
C     (1)J. L. ROUTBORT, J. C. VOGLEWEDE, AND D. S. WILKINSON,
C        FINAL-STAGE DENSIFICATION OF MIXED OXIDE FUELS, JOURNAL OF
C        NUCLEAR MATERIALS, 80 (1979) PP 348 - 355.
C     (2)A. A. SOLCMON, K. M. COCHRAN AND J. A. HABERMEYER, MODELLING
C        HOT-PRESSING OF UO2, NUREG/CR  - PUR-101.
C
C
C     FHOTPS WAS DEVELOPED AND PROGRAMMED BY R. E. MASON-AUGUST 1977.
C     FHOTPS WAS REVISED BY R. E. MASON  APRIL 1981.
C
C     STANDARD ERROR OF ESTIMATE IS PLUS OR MINUS 0.5% OF THE
C     CALCULATED DENSITY.   THE STANDARD ERROR MUST BE APPLIED
C     EXTERNAL TO THIS FUNCTION ROUTINE.
C
C
      R      = 8.31432
      T      = FTEMP
      P      = HSTRES
      G      = GRNSIZ
C
      X      = ABS(ALOG10(FOM - 1.9999))
      QU     = 9000.0/(EXP((20.0 - 8.0*X)/X) + 1.0) + 36294.4
      IF(COMP .GT. 0.0) GO TO 20
C
      FHOTPS = 48939.*((1. - RO)/RO)**2.7* P*EXP(-QU/T)/(T*G*G)
      GO TO 30
C
   20 CONTINUE
      FHOTPS = 1.8CE7*((1.-RO)/RO)**2.25*P*EXP(-450000./(R*T))/(T*G*G)
   30 CONTINUE
C
      RETURN
      END
```

9.5 References

A-9.1. A. A. Solomon, K. M. Cochran, J. A. Habermeyer, Modeling Hot-Pressing of UO_2, NUREG/CR-PUR-2023, March 1981.

A-9.2. J. L. Routbort, J. C. Voglewede, D. S. Wilkinson, "Final-Stage Densification of Mixed Oxide Fuels," Journal of Nuclear Materials,80, 1979 pp. 348-355.

A-9.3. D. S. Wilkinson and M. F. Ashby, "The Development of Pressure Sintering Maps," Proceedings of the Fourth International Conference on Sintering and Related Phenomena, May 26-28, 1975.

A-9.4. D. S. Wilkinson and M. F. Ashby, "Pressure Sintering by Power Law Creep," Acta Metallurgica, 23, November 1975.

A-9.5. R. A. Wolfe and S. F. Kaufman, Mechanical Properties of Oxide Fuels (LSBR/LWB) Development Program, WAPD-TM-58, October 1967.

A-9.6. R. C. Rossi and R. M. Fulrath, "Final Stage Densification in Vacuum Hot-Pressing of Alumina," Journal of the American Ceramic Society, 48, 1965, pp. 558-564.

A-9.7. J. D. McCelland, Kinetics of Hot Pressing, NAA-SR-5591, 1961.

A-9.8. G. M. Fryer, "Hot Pressing of Alumina: A New Treatment of Final Densification," Trans. Brit. Ceram. Soc. 66, 1967 pp. 127-134.

A-9.9. M. S. Seltzer, A. H. Claver, B. A. Wilcox "The Influence of Stoichiometry on Compression Creep of Uranium Dioxide Single Crystals, Journal of Nuclear Materials,44, 1972, pp. 43-56.

A-9.10. M. S. Seltzer, J. S. Perrin, A. H. Clauer, B. A. Wilcox, "A Review of Creep Behavior of Ceramic Nuclear Fuels," Reactor Technology, 14, No. 2, January 1971, pp. 99-135.

A-9.11. M. S. Seltzer, A.H. Claver, B. A. Wilcox, "The Stress Dependence for High Temperature Creep of Polycrystalline Uraniam Dioxide," Journal of Nuclear Materials, 34, 1970, pp. 351-353.

A-9.12. S. F. Kaufman, The Hot-Pressing Behavior of Sintered Low-Density Pellets of UO_2, ZrO_2-UO_2, ThO_2 and ThO_2-UO_2, WAPD-TM-751, May 1969.

A-9.13. I. Amato, R. L. Colombo, A. M. Petruccioli Balzari, "Hot Pressing of Uranium Dioxide," Journal of Nuclear Materials, 20, 1966, pp. 210-214.

A-9.14. P. E. Hart, "Fabrication of High-Density UO_2 and $(U_{0.75}Pu_{0.25})O_2$ by Hot Pressing," Journal of Nuclear Materials, 51, 1974, pp. 199-202.

A-9.15. I. H. Waren and A. C. D. Chaklader "Reactive Hot Pressing of Nonsticniometric Uranium Dioxide," Metallurgical Transactions, 1, 1970, pp. 199-205.

A-9.16. J. C. Voglewede, Reactor Development Program Progress Report, ANL-RDP-26, March 1974.

A-9.17. J. C. Voglewede, Reactor Development Program Progress Report, ANL-RDP-29, June 1974.

A-9.18. D. L. Hagrman, G. A. Reymann, R. E. Mason, MATPRO-Version Revision 1: A Handbook of Materials Properties for Use in Analysis of Light Water Reactor Fuel Rod Behavior, NUREG/CR-0497, TREE-1280, Rev. 1, February 1980.